






Circulating galectin-1 delineates response to bevacizumab in melanoma patients and reprograms endothelial cell biology

Nadia Bannoud^{a,1}, Juan C. Stupirski^{b,1}, Alejandro J. Cagnoni^{b,c,1} , Pablo F. Hockl^b, Juan M. Pérez Sáez^b, P. Alfredo García^a, Yamil D. Mahmoud^{b,d}, Julián Gambarte Tudela^a, Marco A. Scheidegger^b, Andrea Marshall^e, Pippa G. Corrie^f, Mark R. Middleton^g, Karina V. Mariño^c , M. Romina Girotti^{b,d,2}, Diego O. Croci^{a,3} , and Gabriel A. Rabinovich^{b,h,3,4}

Contributed by Gabriel A. Rabinovich; received August 21, 2022; accepted December 6, 2022; reviewed by Arjan Griffioen and Ignacio Melero

Blockade of vascular endothelial growth factor (VEGF) signaling with bevacizumab, a humanized anti-VEGF monoclonal antibody (mAb), or with receptor tyrosine kinase inhibitors, has improved progression-free survival and, in some indications, overall survival across several types of cancers by interrupting tumor angiogenesis. However, the clinical benefit conferred by these therapies is variable, and tumors from treated patients eventually reinitiate growth. Previously we demonstrated, in mouse tumor models, that galectin-1 (Gal1), an endogenous glycan-binding protein, preserves angiogenesis in anti-VEGF-resistant tumors by co-opting the VEGF receptor (VEGFR)2 signaling pathway in the absence of VEGF. However, the relevance of these findings in clinical settings is uncertain. Here, we explored, in a cohort of melanoma patients from AVAST-M, a multicenter, open-label, randomized controlled phase 3 trial of adjuvant bevacizumab versus standard surveillance, the role of circulating plasma Gal1 as part of a compensatory mechanism that orchestrates endothelial cell programs in bevacizumab-treated melanoma patients. We found that increasing Gal1 levels over time in patients in the bevacizumab arm, but not in the observation arm, significantly increased their risks of recurrence and death. Remarkably, plasma Gal1 was functionally active as it was able to reprogram endothelial cell biology, promoting migration, tubulogenesis, and VEGFR2 phosphorylation. These effects were prevented by blockade of Gal1 using a newly developed fully human anti-Gal1 neutralizing mAb. Thus, using samples from a large-scale clinical trial from stage II and III melanoma patients, we validated the clinical relevance of Gal1 as a potential mechanism of resistance to bevacizumab treatment.

galectin-1 | angiogenesis | inflammation | cancer therapy | survival

The rapidly rising incidence of cutaneous melanoma has led to an increased number of patients with regional positive lymph nodes (stage III disease) being diagnosed each year (1). Fewer than 50% of patients with resected locoregional melanoma survive to 5 y. Recurrence at 5 y has been reported in 37% of patients with stage IIIA disease, 68% for IIIB disease, and 89% for patients with stage IIIC disease (2). Progress in immunostimulatory and targeted therapies has provided substantial improvement in response rates and has transformed the clinical management of patients (3). In addition, angiogenesis has been proposed as a relevant target for melanoma therapy based on preclinical studies and clinical trials (4). This process is initiated by tumor, stromal, and endothelial cell (EC) secretion of factors such as the vascular endothelial growth factor (VEGF), which is overexpressed in melanoma (5, 6). In addition, many proangiogenic mediators, including VEGF, also show immunoregulatory activity (7), suggesting that blockade of these pathways may function by suppressing aberrant angiogenesis and enhancing antitumor T cell responses.

It has been shown that VEGF levels measured in either tumor tissue or plasma of melanoma patients correlate with disease stage and tumor burden and might have prognostic significance (5, 6, 8–10). Antiangiogenic therapies using bevacizumab, a monoclonal antibody (mAb) that targets VEGF, have provided survival gains for patients with some types of advanced cancer (11). In the adjuvant setting, VEGF blockade after surgery has been shown to prevent the spread of the disease (5). Additionally, results from clinical trials of bevacizumab activity in patients with advanced melanoma have shown promising efficacy (12, 13). A phase 3 clinical study named Avastin in melanoma (AVAST-M) has tested the efficacy of adjuvant bevacizumab versus observation after resection of melanoma to establish whether angiogenesis inhibition would offer clinical benefit in patients at high risk of recurrence (14, 15). This multicenter, open-label, randomized controlled phase 3 trial of adjuvant bevacizumab versus standard surveillance involved 1,343 patients with resected American Joint Committee on Cancer (AJCC) stage IIB, IIC, and III cutaneous melanoma who were randomized to receive either adjuvant bevacizumab

Significance

Translating preclinical success of VEGF-targeted therapies into clinical practice has been challenging due to development of resistance mechanisms and lack of reliable biomarkers of treatment response. Here, we show that galectin-1 (Gal1), a β -galactoside-binding lectin with proangiogenic and immunoregulatory activities, is elevated in plasma from bevacizumab-treated melanoma patients participating in AVAST-M, a phase 3 clinical trial of adjuvant bevacizumab versus standard surveillance. Notably, increasing Gal1 levels over time enhance the risk of recurrence and death only in patients in the bevacizumab arm. Using a newly developed fully human anti-Gal1 antibody, we demonstrated that circulating Gal1 was functionally active as it was able to reprogram endothelial cell biology. Thus, changes in plasma Gal1 levels may delineate resistance to VEGF-targeted therapies.

Reviewers: A.W.G., Vrije Universiteit Amsterdam; and I.M., Universidad de Navarra.

Copyright © 2023 the Author(s). Published by PNAS. This article is distributed under [Creative Commons Attribution-NonCommercial-NoDerivatives License 4.0 \(CC BY-NC-ND\)](https://creativecommons.org/licenses/by-nc-nd/4.0/).

¹N.B., J.C.S., and A.J.C. contributed equally to this work.

²Present address: Universidad Argentina de la Empresa, Instituto de Tecnología, Buenos Aires, Argentina.

³D.O.C. and G.A.R. should both be considered senior authors.

⁴To whom correspondence may be addressed. Email: gabyrabi@gmail.com.

This article contains supporting information online at <https://www.pnas.org/lookup/suppl/doi:10.1073/pnas.2214350120/-/DCSupplemental>.

Published January 12, 2023.

(7.5 mg/kg i.v. once every 3 wk for 1 y) or standard observation. The primary end point was detection of an 8% difference in the 5-y overall survival (OS) rate, while the secondary end points included disease-free interval (DFI) and distant metastasis-free interval (DMFI). The interim analysis and the 5-y follow-up revealed an improvement in DFI but not in OS for patients in the bevacizumab arm compared with those in the observational arm (14, 15).

Galectins, a family of soluble glycan-binding proteins, are multifunctional players of different hallmarks of cancer, triggering both glycan-dependent and glycan-independent regulatory circuits in the tumor microenvironment (TME) (16). Galectin-1 (Gal1), a prototype member of this family, has emerged as a critical mediator of resistance to different therapeutic modalities, including chemotherapy, radiotherapy, targeted therapy, immunotherapy, and antiangiogenic therapy (17–21). Mechanistically, Gal1 can reprogram the vascular and immune landscapes of tumors through intracellular and extracellular mechanisms. Within the immune compartment, Gal1 is up-regulated during activation (22, 23) and modulates T cell survival (24), cytokine production (25, 26), regulatory T (Treg) cell expansion (27, 28), and dendritic cell immunogenicity (29). By fostering these immunoregulatory programs, Gal1 confers immune privilege to melanoma cells (30, 31). Additionally, Gal1 expressed by cancer, endothelial, or stromal cells promotes angiogenesis in a variety of tumor types (19, 32–34). Mechanistically, Gal1 binds to complex N-glycans on VEGFR2 and neuropilin (NRP-1) and activates VEGF-like signaling on ECs (19). Interestingly, hypoxic and immunosuppressive conditions induce remodeling of the EC surface glycome and regulate both Gal1 binding to ECs and Gal1 upregulation in human and mouse melanoma cells (19, 34). On the basis of its selective binding to N-glycans on VEGFR2, we demonstrated that Gal1 preserves angiogenesis in VEGF blockade settings (19, 35, 36). Disruption of the Gal1–N-glycan axis restrained growth of a variety of tumor types including melanoma by promoting vascular remodeling and favoring influx of immune cells into tumor sites (19). These results demonstrated a central role of Gal1 as a molecular driver underlying resistance to anti-VEGF therapy in preclinical models. However, the clinical implications of these findings are not clear. In this regard, anti-galectin (Gal1, Gal3, and Gal9) antibodies have been detected in plasma from melanoma patients treated with bevacizumab combined with ipilimumab (anti-CTLA-4 mAb) (37, 38).

In this study, we explored the relevance of circulating Gal1 in plasma of bevacizumab-treated melanoma patients, highlighting its association with disease recurrence and risk of death and emphasizing its central role in reprogramming EC biology.

Results

Relevance of Gal1 Expression at Baseline in Predicting OS or DFI in Bevacizumab-Treated Patients. To study the relevance of Gal1 in predicting response to anti-VEGF treatment, we first analyzed basal circulating levels of this lectin in a total of 189 stage II and III melanoma patients from the AVAST-M trial (14, 15). Baseline Gal1 levels were analyzed in plasma samples from 94 patients in the bevacizumab arm and 95 patients in the observation arm. The characteristics were similar among all participants in the trial (Table 1) (15). Of these 189 patients, 68 patients had died (36%), and 95 had recurred (50%). The median Gal1 level at baseline for all 189 patients was 29.4 ng/mL [interquartile range (IQR), 22.5 to 40.1 ng/mL; range, 7.7 to 153.2 ng/mL]. Differences in baseline Gal1 levels were not considerably different across trial arms [median 27.6 (IQR, 21.5 to 35.5) for those in

Table 1. Disease characteristics (primary tumor Breslow thickness, primary tumor ulceration status, disease stage, BRAF status, trial arm, years between diagnosis and randomization, class, and patient sex) classified according to low, medium, or high Gal1 expression

Tumor feature	Low Gal1	Medium Gal1	High Gal1	Total
N	48	93	48	189
Breslow thickness, mm				
<2	13 (27%)	24 (26%)	19 (40%)	56 (30%)
>2-4	13 (27%)	36 (39%)	6 (12%)	55 (29%)
>4	21 (44%)	29 (31%)	19 (40%)	69 (36%)
Unknown	1 (2%)	4 (4%)	4 (8%)	9 (5%)
Ulceration				
Present	26 (54%)	40 (43%)	18 (37%)	84 (44%)
Absent	17 (36%)	40 (43%)	20 (42%)	77 (41%)
Unknown	5 (10%)	13 (14%)	10 (21%)	28 (15%)
Disease stage				
II	19 (40%)	30 (32%)	15 (31%)	64 (34%)
III (N1a and N2a)	12 (25%)	20 (22%)	8 (17%)	40 (21%)
III (other N)	17 (35%)	43 (46%)	25 (52%)	85 (45%)
BRAF status				
BRAF mutation	20 (42%)	32 (34%)	22 (46%)	74 (39%)
BRAF wild type	28 (58%)	61 (66%)	26 (54%)	115 (61%)
Trial arm				
Bevacizumab	27 (56%)	51 (55%)	16 (33%)	94 (50%)
Observation	21 (44%)	42 (45%)	32 (67%)	95 (50%)
Years between diagnosis and randomization				
Median (interquartile range)	0.37 (0.28–1.04)	0.44 (0.32–1.54)	0.47 (0.33–1.63)	0.44 (0.32–1.53)
Range	0.15–16.11	0.11–18.34	0.18–17.97	0.11–18.34

the bevacizumab arm and median 33.0 (IQR, 24.6 to 43.4) for those in the observation arm]. Moreover, Gal1 levels were not statistically different between patients (N = 74) who had tumors with BRAF mutation (median, 27.9; IQR, 22.3 to 42.4) and patients (N = 115) with BRAF wild-type (WT) tumors (median, 29.6; IQR, 22.6 to 38.4; $P = 0.64$).

For the 189 patients presenting baseline Gal1 detection, higher Gal1 levels were associated with a considerable reduction in the risk of recurrence (hazard Ratio (HR) = 0.91 per 5-unit increase; 95% CI, 0.85 to 0.98), and there was a trend toward a reduction in their risk of death (HR = 0.93 per 5-unit increase; 95% CI, 0.86 to 1.01; $P = 0.08$). However, there was no significant interaction between baseline Gal1 levels and the trial arm in predicting DFI ($P = 0.69$) or OS ($P = 0.77$). Of note, there was a significant difference in the risk of recurrence between baseline Gal1 expression grouped into low (<22.5 ng/mL), medium (22.5 and 40 ng/mL), and high (>40 ng/mL) levels (Fig. 1A; $P = 0.006$). Patients with high levels of Gal1 at baseline (HR = 0.43; 95% CI, 0.24 to 0.75), as well as those displaying medium levels (HR = 0.57; 95% CI, 0.36 to 0.90), had a reduced risk of recurrence compared with

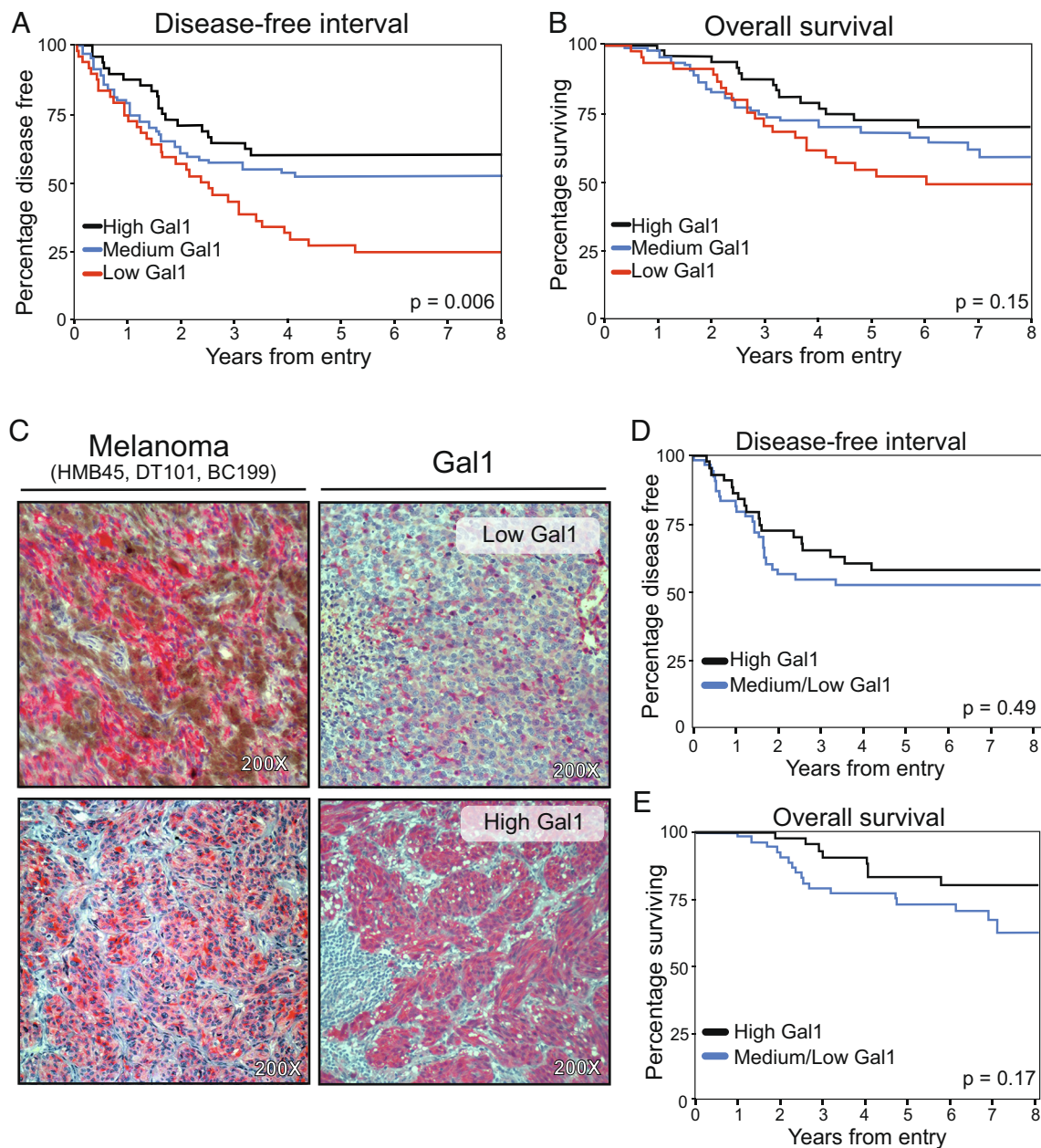


Fig. 1. Relevance of Gal1 expression at baseline in predicting OS or DFI in bevacizumab-treated patients. (A, B) The Kaplan-Meier plot depicting disease-free interval (A) and overall survival (B) of melanoma patients classified according to Gal1 levels (high, medium, or low) as determined by ELISA at baseline. (C) Immunohistochemical (IHC-AP red staining) analysis of pan-melanoma cell markers and Gal1 expression. Representative pan-melanoma cell markers (HMB45, DT101, and BC199) staining (left) and medium/low or high Gal1 levels (right) in tumor tissue from melanoma patients. (D, E) The Kaplan-Meier analysis showing disease-free interval (D) and overall survival (E) of melanoma patients classified according to an IHC score in high or medium/low Gal1 expression at baseline. *P* values are shown in the figure.

those with low levels. However, OS did not differ significantly with regard to Gal1 levels between different groups analyzed (Fig. 1B; $P = 0.15$). Although patients with high levels of Gal1 at baseline (HR = 0.52; 95% CI, 0.26 to 1.01) and those showing medium levels (HR = 0.71; 95% CI, 0.41 to 1.22) presented a trend to have a reduced risk of death compared with those with low levels, there was no significant interaction between Gal1 and the trial arm for DFI ($P = 0.25$) or OS ($P = 0.67$).

To analyze the relevance of Gal1 expression in tumor tissue, we evaluated by immunohistochemistry (IHC) tumors from 96 patients (50 patients in the bevacizumab arm and 46 in the observation arm), of whom 43 (45%) had recurred, and 25 (26%) had died. Samples analyzed included 81 tumor blocks from primary tumors, 10 from lymph node dissections, and five from local recurrences only. All

tissues were composed of melanoma cells as confirmed by immunostaining (Fig. 1C). The median Gal1 score from the 96 patients was five (IQR, 4 to 6; range, 0.5 to 7.0). After categorizing Gal1 scores into medium/low and high using a cut point of five, there was no significant difference in DFI (HR = 0.81; 95% CI, 0.44 to 1.48; $P = 0.49$; Fig. 1D) or OS (HR = 0.55; 95% CI, 0.24 to 1.28; $P = 0.17$; Fig. 1E) between groups showing different expression of this lectin. Notably, there was no significant interaction between Gal1 groups and the trial arm for DFI ($P = 0.74$) or OS ($P = 0.28$).

Increased Gal1 Levels over Time Are Associated with Higher Risk of Disease Recurrence and Lower OS in Bevacizumab-Treated Patients. From samples obtained during the AVAST-M trial, we were able to determine Gal1 levels at baseline and other time points

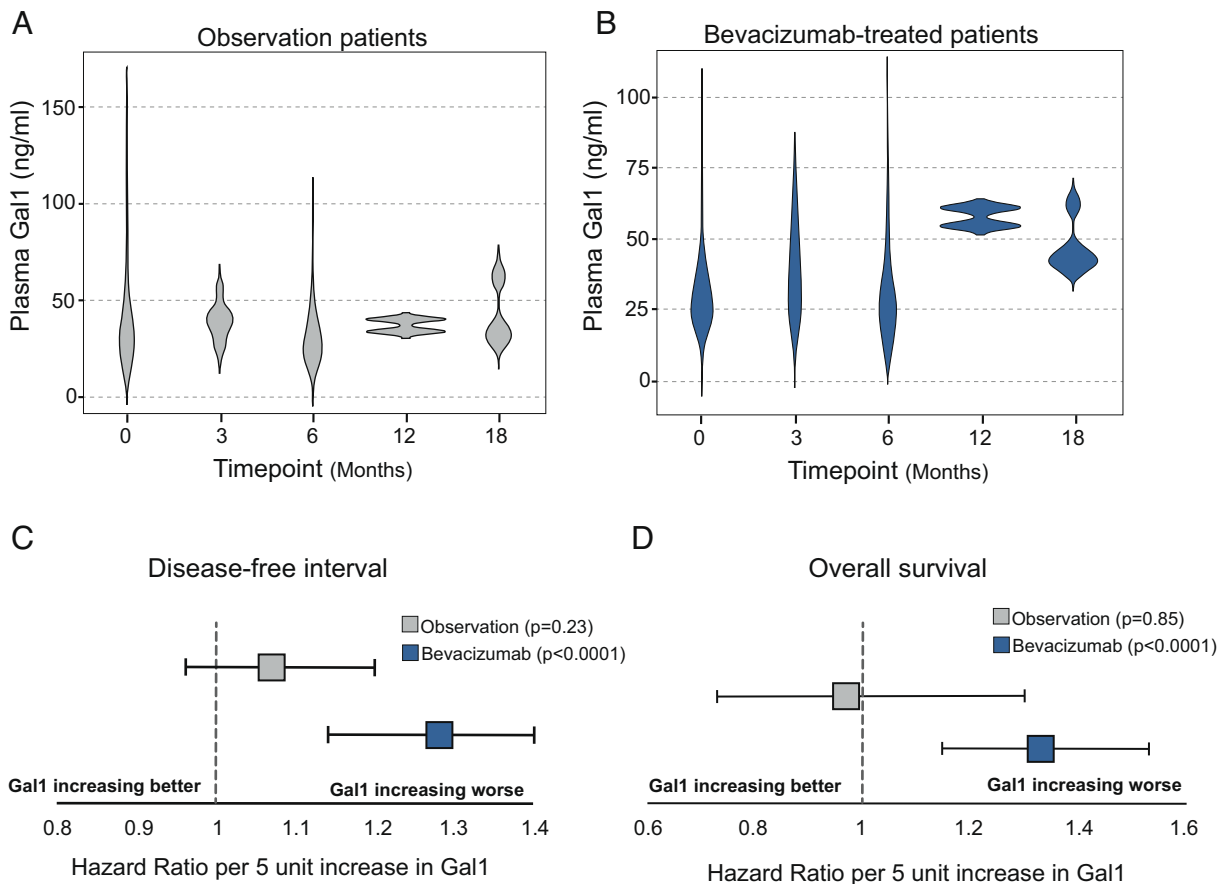


Fig. 2. Increasing Gal1 levels over time are associated with higher risk of disease recurrence and lower OS in bevacizumab-treated patients. (A and B) Violin plots depicting Gal1 expression levels in plasma from melanoma patients in the observation (A) and bevacizumab-treated (B) arms. (C and D) Hazard ratio plots showing the association of increasing Gal1 levels on bevacizumab-treated melanoma patients over time on DFI (C) and OS (D) by the trial arm. *P* values are shown in the figure.

in 94 patients. Of those, 28 (30%) had recurred, and 19 (20%) had died. The distribution of Gal1 levels over time by the trial arm is shown in Fig. 2 A and B. Notably, increasing Gal1 levels over time were associated with a considerable increase in the risk of recurrence (HR = 1.14 per 5-unit increase; 95% CI, 1.06 to 1.22; *P* = 0.0003). Moreover, there was a significant interaction between Gal1 levels over time and the trial arm for DFI (*P* = 0.02). The risk of recurrence was significantly higher with increasing Gal1 levels over time for patients in the bevacizumab arm (HR = 1.28 per 5-unit increase; 95% CI, 1.14 to 1.44; *P* < 0.0001) but not for those in the observation arm (HR = 1.07 per 5-unit increase; 95% CI, 0.96 to 1.20; *P* = 0.23; Fig. 2C). Likewise, increasing Gal1 levels over time were also associated with increased risk of death (HR = 1.20 per 5-unit increase; 95% CI, 1.08 to 1.32; *P* = 0.0005). Consistently, there was a significant interaction between Gal1 levels over time and the trial arm for OS (*P* = 0.05). Increasing Gal1 levels over time significantly increased the risk of death for patients in the bevacizumab arm (HR = 1.33 per 5-unit raised; 95% CI, 1.15 to 1.53; *P* < 0.0001) but not for those in the observation arm (HR = 0.97 per 5-unit increase; 95% CI, 0.73 to 1.30; *P* = 0.85; Fig. 2D).

Of these 94 patients, 19 had an increase of 1.5-fold or more in Gal1 levels over time (11 in the bevacizumab arm and 8 in the observation arm), and of these, 16 (84%) had recurred; 8 within 1 mo of Gal1 measurement, and 9 had died (47%). Of the remaining 75 patients, only 12 (16%) had recurred, and 10 had died (13%). Patients with a 1.5-fold increase in Gal1 levels over time had a significantly higher risk of recurrence than those without (HR = 20.34; 95% CI, 9.49 to 43.59; *P* < 0.0001) and also showed

higher risk of death (HR = 5.09; 95% CI, 2.06 to 12.55; *P* = 0.0004). Of note, we could not find a significant interaction between patients displaying a 1.5-fold increase in Gal1 levels over time and the trial arm for both DFI (*P* = 0.19) and OS (*P* = 0.31). Supporting these findings in another tumor type, bioinformatic analysis of a dataset of glioblastoma patients responding (*N* = 6) or not (*N* = 10) to treatment with bevacizumab in combination with irinotecan (39) revealed an increase in *LGALS1* gene expression following treatment only in the nonresponding group (*P* = 0.0121) (SI Appendix, Fig. S1). Thus, changes in Gal1 levels over time delineate response to bevacizumab, suggesting a role of Gal1 in adaptive resistance to VEGF blockade.

Newly Developed Anti-Human Gal1 mAb Reprograms EC Biology.

In order to validate the functional relevance of human circulating Gal1 in plasma from melanoma patients, and further evaluate the relevance of this lectin as a potential therapeutic target, we generated a fully human anti-Gal1 neutralizing mAb. After preliminary screening, two clones, named mAb-21 and mAb-42, were selected based on their ability to block the interaction between Gal1 and *N*-acetyllactosamine (LacNAc) measured by isothermal titration calorimetry (ITC) assays (Fig. 3A). Remarkably, incubation with mAb-21 or mAb-42 resulted in 50% inhibition of Gal1 binding to LacNAc (Fig. 3A). Further evaluation of the affinity of mAb-21 and mAb-42 was performed by surface plasmon resonance (SPR) assays toward covalently immobilized human recombinant Gal1 (rGal1) (Fig. 3B). Association and dissociation curves were fitted with a 1:1 kinetic interaction model and the association (k_{on}) and

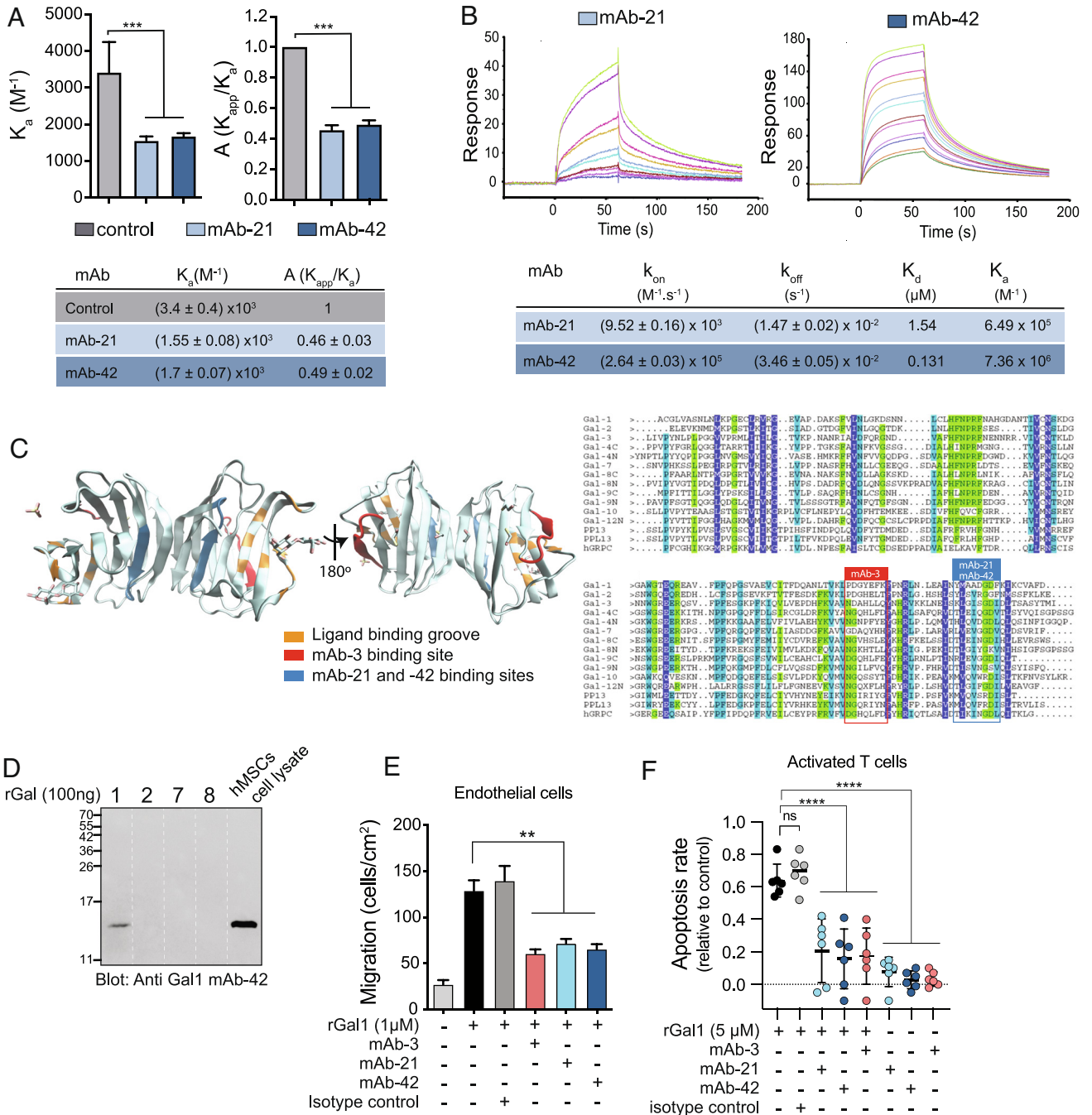


Fig. 3. Biochemical and functional characterization of fully human neutralizing anti-Gal1 mAbs. (A) ITC inhibition assay. LacNAc solution was titrated into a sample cell containing human rGal1 in the presence or absence of mAb-21 or mAb-42. Inhibitory A factor was determined as a ratio between the LacNAc-Gal1 affinity constant in the presence (K_{app}) or in the absence (K_a) of the mAbs. (B) Determination of the kinetics (k_{on} and k_{off}) and thermodynamic (K_d and K_a) constants for anti-Gal1 mAb-21 and mAb-42 interaction with rGal1 by SPR. (C) (Left) 3D structure of human Gal1 illustrating the ligand-binding groove and binding epitopes for mAbs. (Right) Sequence alignment of the human galectin family members illustrating epitope recognition regions of mAb-21 and mAb-42 (highlighted in blue) and the previously described mouse anti-Gal1 mAb-3 (highlighted in red). (D) Western blot analysis of the immunoreactivity of anti-Gal1 mAb (mAb-42) with rGal1, rGal2, rGal7, rGal8, and cell lysates from human mesenchymal stem cells (hMSCs). (E) HUVEC migration induced by rGal1 (1 μM) in the presence or absence of human anti-Gal1 neutralizing mAbs or isotype control (10 $\mu g/mL$). (F) Apoptosis of anti-CD3/CD28 mAb-activated T cells exposed or not to 5 μM rGal1 in the absence or presence of different anti-Gal1 blocking mAbs (10 $\mu g/mL$) or isotype control. (A, E, and F) $***P < 0.01$ and $****P < 0.001$. Data represent mean \pm SEM (A, E, and F) or are representative (B and D) of three independent experiments.

dissociation (k_{off}) rates, as well as affinity (K_a) and dissociation (K_d) constants were determined. Notably, mAb-42 showed the highest affinity toward human Gal1 with a K_d constant value of 0.13 μM , consistent with a fast association ($k_{on} = 2.64 \times 10^5 M^{-1} \cdot s^{-1}$) (Fig. 3B). On the other hand, mAb-21 showed 10-fold weaker affinity for Gal1 than mAb-42 ($K_d = 1.54 \mu M$).

Conformational epitope mapping of mAb-21 and mAb-42 was performed by peptide microarray analysis. Both mAbs showed a strong response against epitope-like spot patterns formed by adjacent Gal1 peptides within the consensus motif YMAADGDF, with higher spot intensities detected with increasing peptide length (SI Appendix, Fig. S2A). Epitope sequence YMAADGDF corresponds

to amino acid residues 120 to 127, located on the S2 strand of the concave S-sheet, next to subsite A of the carbohydrate ligand-binding group (Fig. 3C). The identity of this epitope sequence was further validated by epitope substitution scan analysis in which similar heat maps were observed for both mAbs, highlighting a conserved core motif ¹²⁰YMAADGDF¹²⁷ and a variable stretch ¹¹⁵LEAIN¹¹⁹ (SI Appendix, Fig. S2B). This epitope sequence differs from the one recognized by our previously generated mouse anti-Gal1 mAb-3 (40). Interestingly, epitopes recognized by mAb-21 and mAb-42 were only present in Gal1 protein, but not in other human galectins, thus emphasizing their specificity (Fig. 3C). In line with computational predictions, immunoblot analysis further validated immunoreactivity of mAb-42, which selectively recognized Gal1, but not other members of the galectin family such as Gal2, Gal7, or Gal8 (Fig. 3D). Moreover, human anti-Gal1 mAbs, but not an isotype control, showed functional blocking activity as they successfully inhibited migration of human umbilical vein ECs (HUVECs) induced by human rGal1 as previously observed with a mouse anti-Gal1 mAb (40) (Fig. 3E). Given the proapoptotic activity of Gal1, the neutralizing capacity of mAb-21 and mAb-42 was confirmed in T cell apoptosis assays (Fig. 3F). Collectively, these results highlight the high affinity, specificity, and neutralizing capacity of two human anti-Gal1 mAbs.

Plasma from Bevacizumab-Treated Nonresponding Patients Reprograms EC Biology through the Gal1-VEGFR2 Pathway.

Given the increased levels of Gal1 over time in patients treated with bevacizumab, and their association with risks of recurrence and death, we investigated whether plasma Gal1, particularly in the bevacizumab arm, may actively promote angiogenesis, thus compensating for the absence of VEGF. We analyzed the proangiogenic capacity of plasma samples from melanoma patients enrolled in the bevacizumab arm at baseline and 6 or 12 mo after treatment. Supporting the contribution of Gal1 to the proangiogenic capacity of plasma samples, Gal1 levels strongly correlated with the ability of plasma to induce EC migration (Fig. 4A). Interestingly, neutralizing Gal1 activity, using the anti-Gal1 mAb-42, partially inhibited migration of HUVECs induced by the most highly proangiogenic samples (Fig. 4B). Moreover, Gal1 neutralization also blunted HUVEC tubulogenesis induced by plasma samples from melanoma patients in the bevacizumab arm (Fig. 4C), highlighting the contribution of this lectin to the proangiogenic activity of human plasma from melanoma patients.

Next, we analyzed the proangiogenic capacity of plasma samples over time following bevacizumab treatment in the absence or presence of anti-Gal1 blocking mAb. As mentioned above, Gal1 levels in plasma samples increased gradually during bevacizumab treatment, suggesting that higher levels of Gal1 may compensate for the absence of VEGF, preserving the angiogenic phenotype of bevacizumab-treated tumors. Although Gal1 blockade at baseline did not significantly impair migration of HUVECs induced by plasma samples (Fig. 4D), probably because VEGF primarily contributed to this effect, neutralizing Gal1 after bevacizumab treatment using anti-Gal1 mAb-42 substantially decreased the proangiogenic capacity of plasma samples (Fig. 4D and E). Interestingly, reduced HUVEC migration was also observed when these cells were exposed to plasma samples in the presence of axitinib, a receptor tyrosine kinase inhibitor that preferentially suppresses VEGFR signaling (Fig. 4D), thus substantiating the contribution of these RTKs to this pathway (19). Accordingly, in a HUVEC spheroid sprout assay, plasma from patients treated with bevacizumab showed sustained proangiogenic activity over time, and this effect was impaired in the presence of the anti-Gal1

mAb-42 (Fig. 4E). Interestingly, this uncompromised proangiogenic capacity under bevacizumab treatment suggests that a Gal1-dependent compensatory mechanism is triggered in response to VEGF blockade.

To gain further insights into the mechanisms underlying angiogenesis induced by plasma Gal1, we finally studied the ability of plasma samples to induce VEGFR2 signaling. At baseline, plasma samples from melanoma patients induced VEGFR2 and Erk1/2 phosphorylation at levels similar to those found in HUVECs treated with VEGF (20 ng/mL) (Fig. 4F). Of note, Gal1 blockade did not affect VEGFR2 signaling at this stage. Interestingly, after 6 mo under bevacizumab treatment, plasma samples from melanoma patients still induced VEGFR2 phosphorylation (Fig. 4F). Here, neutralization of Gal1 using mAb-42 partially prevented VEGFR2 phosphorylation induced by plasma samples from bevacizumab-treated melanoma patients. Altogether, these data highlight a major role for Gal1 as a proangiogenic factor released systemically in response to VEGF blockade and suggest the functional role of this lectin in delineating response to VEGF blockade in clinically relevant settings, thus validating our previous findings in anti-VEGF-resistant mouse tumor models (19).

Discussion

Genetic and pharmacological inhibition of vascular signaling pathways has provided important evidence that abnormal angiogenesis is a hallmark of cancer (41). In spite of the complexity of signaling pathways implicated in this process, bevacizumab, a mAb that targets VEGF (42), is the most widely prescribed antiangiogenic drug for multiple solid metastatic cancers (43). Although therapies targeting VEGF have offered significant clinical benefit by improving PFS and OS, several patients experience decreased benefit over time (44). Particularly in melanoma patients, bevacizumab has shown no impact on either OS or PFS and had limited impact on DFI (12, 14, 15), suggesting the contribution of compensatory pathways that preserves angiogenesis in the absence of VEGF signaling.

In this work, using samples from AVAST-M, the larger-scale trial that evaluated the role of bevacizumab in stage II–III melanoma patients (14), we demonstrated that Gal1 is elevated in plasma from nonresponding bevacizumab-treated patients. Despite no significant interactions between Gal1 levels, and OS or DFI responses at baseline, we found that increasing Gal1 levels over time in patients in the bevacizumab arm significantly increased the risks of recurrence and death. Interestingly, these associations were not observed in patients in the observation arm, suggesting that Gal1 may act as a compensatory mechanism that preserves angiogenesis in settings of VEGF blockade. Strikingly, this effect had a different trend when Gal1 was analyzed at baseline, suggesting a central role for this lectin in conferring acquired resistance to VEGF blockade. Accordingly, we previously demonstrated that Gal1 is up-regulated in anti-VEGF-resistant mouse tumors, but not in sensitive mouse tumors 4 and 7 d after treatment, and sustains angiogenesis via a noncanonical glycan-dependent mechanism (19). In this study, we found that elevated Gal1 levels in plasma are associated with angiogenesis in bevacizumab-treated melanoma patients. Specifically, we showed that 6 to 12 mo after bevacizumab treatment, plasma samples from melanoma patients still induced *ex vivo* angiogenesis and VEGFR2 signaling at levels similar to those found at baseline. Interestingly, blockade of Gal1 in those samples prevented HUVEC migration, tube formation, 3D sprouting, and VEGFR2 phosphorylation only in the bevacizumab-treated arm. These results substantiate the role of this lectin in acquired resistance to anti-VEGF

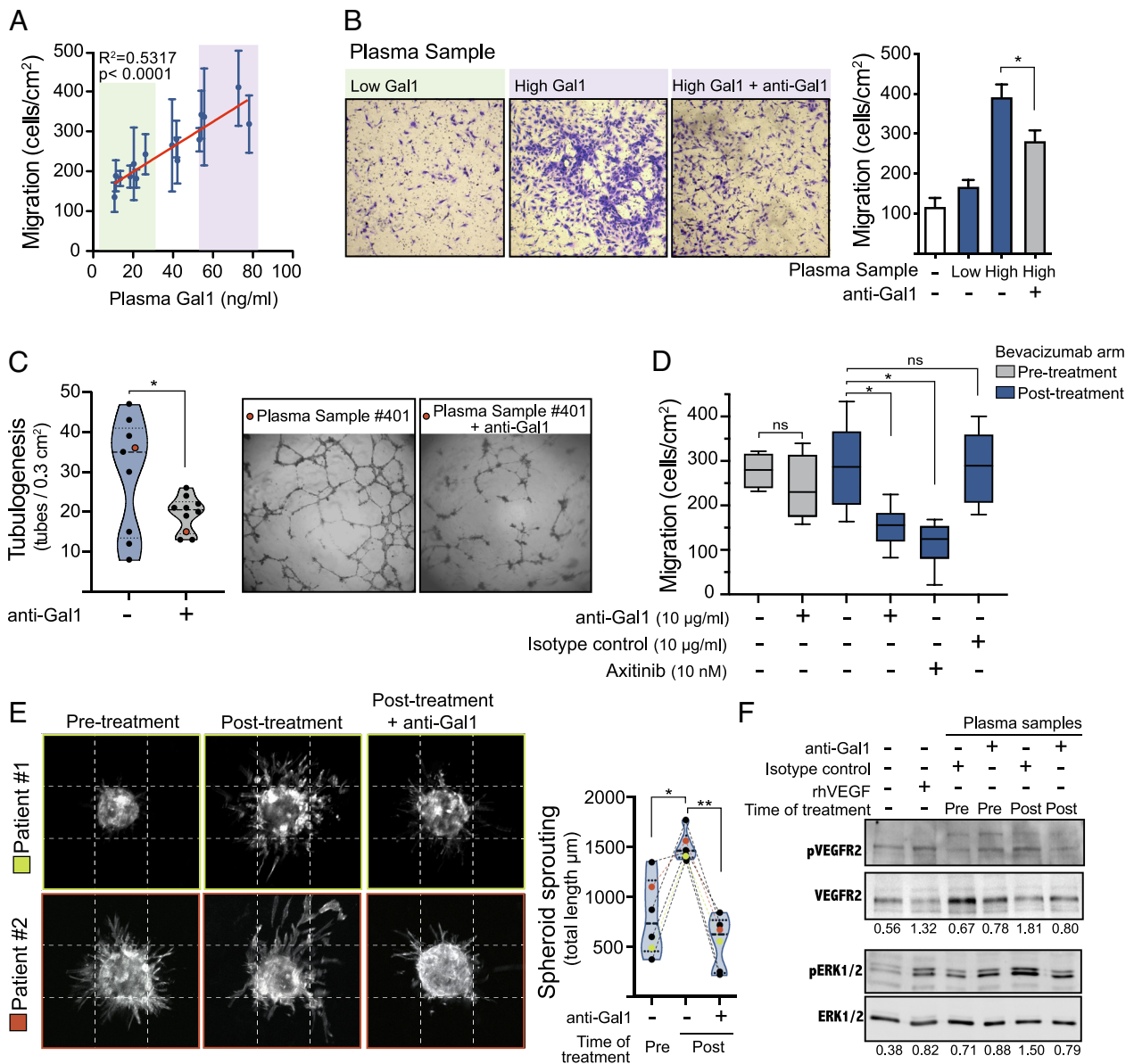


Fig. 4. Circulating Gal1 contributes to the proangiogenic activity of plasma samples from bevacizumab-treated melanoma patients. (A) Association of Gal1 levels and induction of HUVEC migration by plasma samples from melanoma patients. (B) Transwell migration of HUVECs incubated with plasma samples from melanoma patients containing low or high Gal1 levels preincubated or not with the anti-Gal1 mAb-42 (10 µg/mL). Data represent mean ± SEM of eight patient plasma samples. (C) *Left:* analysis of tube formation in HUVECs stimulated with plasma from melanoma patients preincubated or not with anti-Gal1 mAb-42 (10 µg/mL). Violin plots represent the mean and distribution of tube formation from patient plasma samples. *Right:* representative images are shown. (D) HUVEC migration induced by plasma samples from melanoma patients at baseline and after 6-mo treatment with bevacizumab, preincubated or not in vitro with an anti-Gal1 mAb-42 (10 µg/mL), the VEGFR tyrosine kinase inhibitor axitinib (10 nM), or isotype-matched mAb (IgG2κ; 10 µg/mL). Data represent mean ± quartile distribution of migrating cells/cm² per group. (E) Spheroid sprouting assay of HUVECs stimulated for 16 h with plasma samples from melanoma patients at baseline or 6 or 12 mo posttreatment with bevacizumab incubated in vitro with or without anti-Gal1 blocking mAb-42 (10 µg/mL). *Left:* representative images of spheroids from two patient samples. *Right:* quantification of sprout length. Violin plots represent the mean and distribution of spheroid sprouting length from six patients' plasma samples. Colored dots identify patient samples shown in the *Left* images. (F) Representative immunoblot analysis showing phosphorylated and unphosphorylated VEGFR2 and ERK1/2 in HUVECs stimulated with plasma samples from patients at baseline or after 6 mo under bevacizumab treatment in the presence of anti-Gal1 mAb-42 (10 µg/mL) or isotype control. **P* < 0.05 and ***P* < 0.01.

treatment. Notably, inhibition of HUVEC migration was also verified when we exposed these cells to plasma samples in the presence of axitinib, highlighting the contribution of VEGFR tyrosine kinase signaling to these effects. Importantly, in addition to the direct impact of Gal1 on EC biology (19, 33, 34), this lectin could also promote compensatory angiogenesis and resistance to bevacizumab by acting on other cell types including stromal or myeloid cells. Moreover, although increasing levels of Gal1 in patients in the bevacizumab arm, but not in the observational arm, strongly suggest a role of this lectin as a mechanism of resistance to anti-VEGF treatment, other mechanisms might also

contribute to this effect, including an overall increase in tumor burden.

The role of soluble circulating galectins in cancer patients has been previously explored. Plasma levels of Gal2, Gal3, Gal4, and Gal8 have shown a strong correlation with tumor cell adhesion, angiogenesis, and metastasis in breast and colon cancers either through binding to extracellular matrix glycoproteins (45–47) or by promoting the release of cytokines from the vascular endothelium (48). Regarding Gal1, several studies in breast adenocarcinoma (45, 47), Hodgkin lymphoma (49), colorectal cancer (50, 51, 52), renal cell carcinoma (51), high-grade glioma (53),

neuroblastoma (54), oral squamous cell carcinoma (55, 56), thyroid carcinoma (52, 57), lung adenocarcinoma (58), and pancreatic adenocarcinoma (59) indicate that circulating Gal1 levels are clinically relevant, predicting clinical outcome and promoting cancer progression by favoring angiogenesis, immunosuppression, and metastasis. In this sense, galectins have been proposed to function as regulatory checkpoint molecules that simultaneously control immune and vascular programs (60). Notably, most of the studies dedicated to analyzing plasma galectins in cancer patients focused on correlations between galectin levels and patient prognosis (17); however, their functional relevance remains poorly explored. Here, we showed that plasma-soluble Gal1 is indeed functional, being able to reprogram EC biology at concentrations similar to those found in melanoma patients. These findings were validated using a newly developed fully human anti-Gal1 neutralizing mAb.

An essential yet unresolved issue concerning the structure–function relationship of Gal1 is associated with the intrinsic sensitivity of this protein to oxidative microenvironments (61, 62). Given this biochemical limitation, it is still unclear whether this lectin is functionally active in the bloodstream. Here, specific Gal1 blockade impaired the proangiogenic activity of plasma samples from melanoma patients, suggesting the functional integrity of this lectin in the circulation. Although the half-life of circulating galectins is unknown, pioneering studies using truncated Gal3 suggested that galectins remain stable for a few hours in plasma (63). The biological availability of galectins could be increased through binding to serum glycoproteins. In this regard, it has been shown that Gal1 recognizes IgA1 via an interaction with O-glycans (64), thus enhancing its stability by increasing half-life. Furthermore, Gal1 could associate with other soluble glycoproteins such as urokinase-type plasminogen activator, soluble NRP-1, and soluble VEGFRs (35, 65); however, their relevance in modulating half-life of this protein has not been explored. Additionally, Gal1 has been shown to be up-regulated in tumor-derived extracellular vesicles (EVs) (66), which are key regulators of immunosuppression, angiogenesis, metastasis, and drug resistance (67), suggesting a possible role of EVs in sustaining availability of Gal1 in plasma. Whether this lectin is associated with plasma carrier glycoproteins, is protected within EVs, or functions as a free bioactive lectin remains an open question.

The function of Gal1 is highly controlled by the glycosylation status of target cells. In this regard, tumor-associated ECs display remarkable changes on their cell surface glycome, which favor Gal1 binding and signaling in immunosuppressive and proangiogenic microenvironments (19). In this sense, the transcriptional and phenotypical changes of ECs in tumoral versus normal tissue, recently characterized at a single-cell resolution level, support our observations (68). Notably, in culture conditions, HUVECs exhibit a gene expression profile (68) and glycan repertoire (19, 69) similar to that observed in tumor-associated ECs characterized by complex branched N-glycans and decreased α 2,6 sialylation. Thus, Gal1 binding and signaling in the TME may be fine-tuned by environmental factors such as redox status, pH, and the density of Gal1-specific glycan epitopes exposed on target cells, adding complexity to the regulation of Gal1 function. Notwithstanding this, our results and those previously published uphold Gal1 blockade as a rational strategy to inhibit tumor angiogenesis and circumvent resistance to antiangiogenic therapies (19, 32, 34, 70–73).

Interestingly, during this study, we generated, purified, and characterized highly specific fully human anti-Gal1 mAbs (clones 21 and 42), which showed blocking capacity at similar concentrations than those reported for mouse anti-Gal1 mAb (34, 40, 74). Importantly, the new anti-Gal1 mAbs showed high affinity

and specificity for human Gal1 but not for other members of the galectin family.

Based on its dual immunosuppressive and proangiogenic activities, Gal1 arises as a common target of both antiangiogenic and immunotherapeutic modalities, conferring resistance to a broad range of anticancer strategies (17). In this regard, in anti-CD20–treated non–Hodgkin lymphoma, Gal1 has been associated with intrinsic resistance (75). Moreover, Gal1 modulates responses to PD-1 blockade in glioblastoma and HNSC by favoring T cell exclusion (18, 76). Accordingly, we have previously shown that Gal1 blockade promotes CD8 T cell influx and infiltration into the tumor parenchyma (19) and enhances Th1-mediated antitumor responses (27, 29, 30). Furthermore, a previous study from a phase 1 clinical trial in melanoma patients treated with bevacizumab plus ipilimumab revealed the occurrence of anti-galectin (Gal1, Gal3, and Gal9) autoantibodies in response to this combination therapy (37). Particularly, anti-Gal1 autoantibodies correlated with favorable clinical outcomes of these patients (38) and prevailed in those patients treated with bevacizumab plus ipilimumab and not in the ipilimumab arm of the trial, suggesting that anti-Gal1 responses were clinically relevant in the context of VEGF blockade. However, in those studies, samples from patients treated with bevacizumab alone were not tested (38). Thus, Gal1 overexpression may function as an adaptive mechanism that preserves angiogenesis under anti-VEGF treatment. Finally, given the increasing importance of combination therapies in several cancer types and the broad immunosuppressive activity of this lectin, future studies are warranted to investigate whether elevation of plasma Gal1 levels in response to VEGF blockade may also compromise the efficacy of immunotherapeutic strategies.

In conclusion, our findings validate the clinical relevance and functional activity of plasma Gal1 as a potential mechanism of resistance to bevacizumab treatment. Moreover, we describe a newly developed fully human anti-Gal1 mAb capable of inhibiting Gal1 functions with broader therapeutic potential in clinical settings involving dysregulated angiogenesis, including cancer, age-related macular degeneration, and diabetic retinopathy.

Materials and Methods

Patients. The study design, eligibility criteria, stratification variables, and treatment schedules have been described previously (14, 15). Briefly, patients with histological confirmation of completely resected AJCC seventh edition stage IIB, IIC, or IIIA–C cutaneous melanoma were eligible for the trial. The Multicenter Research Ethics Committee and regulatory approvals were obtained as described (14). Written informed consent was obtained from all patients in accordance with the Declaration of Helsinki guidelines. Patients were followed up at least annually for 10 y after randomization. Eligible patients were randomly assigned to adjuvant bevacizumab (7.5 mg/kg i.v. infusion once every 3 wk for one calendar year) or surveillance in a 1:1 ratio, stratified by primary tumor Breslow thickness, N stage, primary tumor ulceration status, and patient sex (Table 1). Randomization occurred within 12 wk of surgical resection. The primary end point of this open-label trial was detection of an 8% difference in the 5-y OS rate, whereas the secondary end points included assessment of DFI.

ELISA. Soluble Gal1 was determined using an in-house Enzyme-Linked Immunosorbent Assay (ELISA) as described (34). In brief, high-binding 96-well microplates (Costar; Corning) were coated with capture Ab (2 μ g/mL purified rabbit anti-human Gal1 polyclonal IgG) in 0.1 M sodium carbonate, pH 9.5. After incubation for 18 h at 4 °C, wells were rinsed three times with wash buffer (0.05% Tween-20 in PBS) and incubated for 1 h at room temperature with blocking solution (2% Bovine Serum Albumin (BSA) in Phosphate buffer saline (PBS)). Samples and standards (100 μ L) were diluted in 1% BSA–Tween-20 and incubated for 18 h at 4 °C. Plates were then washed and incubated with 100 ng/mL biotinylated detection Ab (purified rabbit anti-human Gal1 polyclonal IgG) for 1 h. Plates were rinsed three times before adding 0.33 μ g/mL HRP-labeled streptavidin

(Sigma-Aldrich) for 30 min. After washing, 100 μ L 3,3',5,5'-Tetramethylbenzidine (TMB) solution (0.1 mg/mL tetramethylbenzidine and 0.06% H₂O₂ in citrate-phosphate buffer, pH 5.0) was added to plates. The reaction was stopped by adding 2N H₂SO₄. Optical densities were determined at 450 nm in a Multiskan MS Microplate Reader (Thermo Fisher Scientific). A standard curve ranging from 2.5 to 160 ng/mL human rGal1 was run in parallel.

IHC. Formalin-fixed, paraffin-embedded sections were deparaffinized during 18 h in xylene followed by rehydration essentially as described (34). Heat-mediated antigen retrieval was performed using citrate-based retrieval buffer (10 mM). Samples were blocked in peroxide blocking buffer (3% H₂O₂), followed by blocking buffer (PBS; 1% BSA and 5% normal serum) during 1 h at room temperature. Samples were incubated with HMB45 + M2-7C10 + M2-9E3 anti-melanoma cells Ab (ab732; Abcam) or with anti-Gal1 rabbit polyclonal Ab at 4 °C overnight in a humidified chamber. Then, samples were washed and incubated with a biotinylated secondary Ab (ABC Elite Kit; Vector Laboratories) followed by streptavidin-alkaline phosphatase incubation (ABC-AP Kit; Vector Laboratories). Samples were then washed in PBS, incubated in red chromogen (Vector Red), and counterstained with Mayer's hematoxylin. The Gal1 score was calculated by a semiquantitative assessment of both the intensity of staining (graded as 0 to 3 using adjacent normal parenchyma as reference) and the percentage of positive cells (graded as 0 to 5). Expression levels were categorized as low/medium or high according to the median value of the score.

Generation and Purification of Fully Human Neutralizing Anti-Gal1 mAbs. Anti-Gal1 mAbs were designed, generated, and evaluated by using a contract research service between Creative Biolabs facilities (Shirley) and our facilities at the Institute of Biology and Experimental Medicine (IBYME). Human rGal1 was produced in *Escherichia coli* BL21 (DE3) cells and purified by affinity chromatography on a lactosyl-Sepharose column essentially as described (40) and used to perform two rounds of phage display human single-chain variable fragment (scFv) library panning. After four rounds of screening, 70 clones that bound antigen were selected and assessed by soluble scFv-AP ELISA with rGal1-coated wells. All positive clones were subjected to DNA sequencing. Four sequences were selected and cloned into soluble scFv-AP expression vectors and subjected to soluble scFv expression. The binding and blocking activities of the four scFvs have been evaluated by using competitive inhibition assays in a Nano ITC instrument (TA Instruments). From selected clones, mAb-21 and mAb-42 were converted into full-size mAbs by inserting the variable regions of the scFv into IgG1, kappa-chain mAb sequences. Two pCMV mammalian expression vectors were constructed encoding heavy chain and light chain, respectively, for each mAb. The expression vectors of clones 21 and 42 were transiently transfected and expressed in HEK293 cells. Recombinant human mAbs-21 and mAbs-42 were purified by Protein A affinity chromatography and ultrafiltration and subjected to 0.2-micron sterile filtration (monomer >99%, endotoxin level <0.5 EU/mg, and protein A residual <10 ppm).

Conformational Epitope Mapping. Microarray analysis was performed by PEPperPRINT GmbH (Heidelberg, Germany) as previously described (40). Briefly, mAb-21 and mAb-42 solutions (10 μ g/mL) were incubated with a peptide microarray containing 420 different Gal1 peptides printed in duplicate (840 peptide spots). Samples were analyzed with the LI-COR Odyssey Imaging System scanner, and microarray image analysis was done with the PepSlide® Analyzer. The intensity plots were correlated with peptide and intensity maps, as well as with visual inspection of the microarray scans to identify epitopes that were specifically recognized by the mAb.

Epitope Substitution Scan. Microarray analysis was performed by PEPperPRINT GmbH (Heidelberg, Germany) as previously described (40). Briefly, mAb-21 or mAb-42 solutions (10, 100, and 250 μ g/mL) were incubated in a PEPperCHIP® Peptide Microarray containing 260 different peptides obtained from the exchange of all LEAINYMAADGDF peptide amino acid positions with all 20 main amino acids. Samples were analyzed with the LI-COR Odyssey Imaging System scanner. Microarray image analysis was done with the PepSlide® Analyzer as described above for conformational epitope mapping.

SPR Determinations. SPR affinity studies were performed at the Laboratory of Molecular and Cellular Analytics, SPR (Institute of Humoral Immunity; Faculty of Pharmacy and Biochemistry, University of Buenos Aires) as previously described

(40). Briefly, human rGal1 was covalently immobilized to the Fc2 (active) surface of a CM5 carboxymethyl chip, and the binding of mAb-21 and mAb-42 was evaluated on a Biacore T100 instrument.

ITC Assays. Anti-Gal1 mAb-21 and mAb-42 were evaluated by competitive inhibition assays using ITC. A Nano ITC instrument (TA Instruments) was used for titrations at 298 K. Syringe, cell concentrations and molar ratios, injection volumes, and time intervals between injections varied to obtain sufficient heat production per injection to allow good peak integration and enough time between injections to allow a return to equilibrium. A typical titration involved 20 injections at 3-min intervals of 2.5 μ L aliquots of 2.5 mM LacNAC solution into the sample cell (200 μ L) containing rGal1 (50 μ M) alone or with tested mAb (10 μ M). The syringe and cell solutions were prepared by dissolving LacNAC and rGal1 in a 20 mM phosphate buffer, pH 7.4, and 150 mM NaCl at 298 K. The titration cell was continuously stirred at 300 rpm. The heats of dilution of LacNAC in the buffer were subtracted from the titration data. Inhibitory A factor was determined as a ratio between the LacNAC-Gal1 affinity constant in the presence of the mAb (K_{app}) and the affinity constant without the mAb (K_a). *N*-acetylglucosamine (LacNAC) was purchased from Sigma-Aldrich.

Cell Death Assay. PBMCs from healthy donors were isolated by density gradient centrifugation (Ficoll-Paque), and T cells were activated by incubation with 1 μ g/mL of agonist anti-CD3 and anti-CD28 mAb. After 3 d, cells were washed and incubated in fresh RPMI supplemented with 5% FCS. Next, activated T cells (1.5 \times 10⁵ cells/mL) were incubated with rGal1 (5 μ M) for 6 h in the presence or absence of anti-Gal1 mAbs or isotype control (10 μ M) in RPMI medium supplemented with 5% Fetal Bovine serum (FBS). Cell death was assessed by staining with Fluorescein isothiocyanate (FITC)-conjugated annexin V (BD Biosciences) and propidium iodide (PI) (Sigma) and analyzed on a FACSAria flow cytometer (BD). Results are expressed as the percentage of annexin V⁺ PI⁺ cells.

Isolation of HUVECs. Isolation of HUVECs from umbilical cords was performed essentially as described (77), following approval by the Ethics Committee from the Faculty of Medicine, National University of Cuyo (Mendoza, Argentina) (ref. EXP-CUY: 4693-2018).

EC Migration Assays. HUVECs (3 \times 10⁴/well) were resuspended in supplemented RPMI medium. Cells were placed into the top chamber of 8- μ m pore insert (Millipore), while the bottom well was filled with RPMI 1640 medium containing rGal1 (1 μ M), VEGF (20 ng/mL), or plasma samples obtained from patients at different time periods following bevacizumab treatment. Alternatively, plasma samples from melanoma patients were preincubated for 1 h with human anti-Gal1 mAbs (clone 21 or 42) or isotype control. After 18 to 24 h, inserts were stained with 0.1% crystal violet and 20% methanol solution (Sigma) for 10 min at room temperature. After washing and removal of nonmigrating cells from the top chamber side, inserts were photographed and analyzed in an inverted microscope. For each insert, four images were collected, and cells were counted using Fiji 2.0 software (78).

Immunoblotting. Immunoblotting was performed as described (34). Briefly, equal amounts of rGal1 or protein extracts from HUVECs (30 μ g) exposed to plasma samples preincubated for 1 h with human anti-Gal1 mAbs (clone 21 or 42) or isotype control were resuspended in Laemmli buffer under reducing conditions. Proteins were resolved in 4 to 20% SDS-PAGE and blotted onto nitrocellulose membranes (GE Healthcare). After blocking, the membranes were probed with anti-human Gal1 mAb-21 and mAb-42 (1.5 μ g/mL): anti-VEGFR2 (1/1,000; Cell Signaling), anti-phospho-VEGFR2 (1:1,000; Cell Signaling), anti-ERK-1/2 (1:2,000; Sigma), and anti-phospho-ERK-1/2 (1:1,000; Sigma). Blots were then incubated with horseradish peroxidase (HRP)-labeled anti-human, rabbit, or mouse secondary Ab 1:2,000 (Vector) and developed using the Immobilon Western Chemiluminescent HRP Substrate (Millipore). Protein bands were analyzed with Fiji 2.0 analysis software.

Tubulogenesis Assay. The formation of capillary-like tubular structures was assessed in Geltrex-coated plates as described (77). In brief, HUVECs (1.5 \times 10⁴ cells) were mixed with plasma samples (5% RPMI 1640) from bevacizumab-treated patients at different time points, preincubated or not with anti-Gal1 mAb-42, and then plated on Geltrex-coated 96-well plates at 37 °C for 12 h or, alternatively, on Geltrex-coated μ -slide angiogenesis (Ibidi®) for 6 to 8 h.

Capillary-like tubular structures were visualized by phase-contrast microscopy and recorded by counting the number of tubules (closed areas) per well in a phase-contrast microscope (Nikon E-100).

Spheroid Sprouting Assay. To study angiogenesis in a 3D culture system, a HUVEC spheroid sprouting assay was performed as described (77). Briefly, HUVEC spheroids were obtained by seeding 400 to 500 HUVECs in 100 μ L Methocel spheroid solution (Methocel, FBS, and RPMI 1640 medium in a 20:20:60 ratio and 15 ng/mL VEGF) for 2 to 3 d. Then, spheroids were harvested, washed with PBS, centrifuged (500 \times g for 2 min), and resuspended in Methocel sprouting solution (Methocel and FBS in an 80:20 ratio). Spheroids were mixed with 3 mg/mL type I collagen solution and seeded in a 48-well plate for 30 min at 37 $^{\circ}$ C until collagen gel solidified. Plasma samples from melanoma patients (5% RPMI) preincubated or not for 1 h with human anti-Gal1 mAb (clone 21 or 42) were added on the top of collagen gel. FBS (2%) in RPMI 1640 and FBS (10%) supplemented with 60 ng/mL VEGF in RPMI 1640 were used as negative and positive control, respectively. Sprouting was observed between 12 and 16 h from the initial incubation in an inverted microscope and fixed with PBS containing 4% paraformaldehyde for 1 h at 4 $^{\circ}$ C. Fixation was quenched with 50 mM ammonium chloride for 1 h at RT. Spheroids were permeabilized with 0.2% saponin and 1 mg/mL BSA in PBS for 30 min at RT, and sprouts were visualized by staining F-actin filaments using phalloidin (1:200) for 1 h at RT. Images were obtained in an Olympus FV-1000 confocal microscope and analyzed in Fiji 2.0 software (78). Spheroid sprouting was determined as the average of total sprout length of all viable spheroids in each condition.

Bioinformatic Analysis. Transcriptomic analysis was performed using RNA-seq data obtained from tumor samples of glioblastoma patients before and after treatment with bevacizumab plus irinotecan (responders, $n = 6$; non responders, $n = 10$) (39) (GSE79671). Counts per million (CPMs) were used for statistical analysis.

Statistical Analysis. GraphPad Prism version 8 (GraphPad Software Inc.) was used for statistical analysis. For multiple comparisons, multiple t tests (using the Holm–Sidak correction method), one-way or two-way ANOVA followed by Tukey's or Dunnett's posttest (parametric analysis) or the Kruskal–Wallis test followed

by Dunn's posttest (nonparametric analysis), were used. Kaplan–Meier (survival) curves were compared with the Mantel–Cox (log-rank) test. P values of 0.05 or less were considered significant.

Data, Materials, and Software Availability. All study data are included in the article and/or *SI Appendix*.

ACKNOWLEDGMENTS. This work was supported by grants from Agencia de Investigación, Desarrollo e Innovación (PICT2014-3687 and 2017-0494 to G.A.R., PICT2016-0205 to D.O.C., and PICT2016-2130 to M.R.G./J.M.P.S.), the Bunge and Born Foundation, the Sales Foundation, and The Richard Lounsbery Foundation to G.A.R. We thank Ferioli, Ostry, and Caraballo families for continuous support. The AVAST-M trial was funded by the Cancer Research UK (grant ref. C7535/A6408 and C2195/A8466; ISRCTN81261306; EudraCT Number: 2006-005505-64) and supported by the NIHR Cambridge Biomedical Research Centre (BRC-1215-20014).

Author affiliations: ^aLaboratorio de Glicobiología y Biología Vasculard, Instituto de Histología y Embriología de Mendoza, Consejo Nacional de Investigaciones Científicas y Técnicas, Universidad Nacional de Cuyo, Mendoza 5500, Argentina; ^bLaboratorio de Glicomedicina, Instituto de Biología y Medicina Experimental, Consejo Nacional de Investigaciones Científicas y Técnicas, Buenos Aires 1428, Argentina; ^cLaboratorio de Glicómica Funcional y Molecular, Instituto de Biología y Medicina Experimental, Consejo Nacional de Investigaciones Científicas y Técnicas, Buenos Aires 1428, Argentina; ^dInstituto de Tecnología, Universidad Argentina de la Empresa, Buenos Aires 1073, Argentina; ^eWarwick Clinical Trials Unit, University of Warwick, Coventry CV4 7AL, UK; ^fDepartment of Oncology, Cambridge University Hospitals NHS Foundation Trust, Addenbrooke's Hospital, Cambridge CB2 0QQ, UK; ^gDepartment of Oncology, The University of Oxford, Oxford OX3 7LE, UK; and ^hFacultad de Ciencias Exactas y Naturales, Universidad de Buenos Aires, Buenos Aires 1428, Argentina

Author contributions: N.B., J.C.S., A.J.C., P.F.H., K.V.M., M.R.G., D.O.C., and G.A.R. designed research; N.B., J.C.S., A.J.C., J.M.P.S., P.A.G., Y.D.M., J.G.T., and M.A.S. performed research; P.F.H., J.M.P.S., A.M., P.G.C., and M.R.M. contributed new reagents/analytic tools; N.B., J.C.S., A.J.C., P.F.H., Y.D.M., A.M., P.G.C., M.R.M., K.V.M., M.R.G., D.O.C., and G.A.R. analyzed data; D.O.C., and G.A.R. jointly supervised this work; and M.R.G., D.O.C., and G.A.R. wrote the paper.

Competing interest statement: The authors have patent filings to disclose, P.F.H., J.M.P.S., D.O.C., and G.A.R. are co-inventors in the US Patent 10294295B2: "Methods for modulating angiogenesis of cancers refractory to anti-VEGF treatment."

1. A. M. M. Eggermont, A. Spatz, C. Robert, Cutaneous melanoma. *Lancet* **383**, 816–827 (2014).
2. E. Romano, M. Scordo, S. W. Duszka, D. G. Coit, P. B. Chapman, Site and timing of first relapse in stage III melanoma patients: Implications for follow-up guidelines. *J. Clin. Oncol.* **28**, 3042–3047 (2010).
3. B. Switzer, I. Puzanov, J. J. Skitzki, L. Hamad, M. S. Ernstoff, Managing metastatic melanoma in 2022: A clinical review. *JCO Oncol. Pract.* **18**, 335–351 (2022).
4. B. Basu, S. Biswas, J. Wrigley, B. Sirohi, P. Corrie, Angiogenesis in cutaneous malignant melanoma and potential therapeutic strategies. *Expert Rev. Anticancer Ther.* **9**, 1583–1598 (2009).
5. P. A. Ascierto *et al.*, Prognostic value of serum VEGF in melanoma patients: A pilot study. *Anticancer Res.* **24**, 4255–4258 (2004).
6. S. Ugurel, G. Rapp, W. Tilgen, U. Reinhold, Increased serum concentration of angiogenic factors in malignant melanoma patients correlates with tumor progression and survival. *J. Clin. Oncol.* **19**, 577–583 (2001).
7. S.-J. Li, J.-X. Chen, Z.-J. Sun, Improving antitumor immunity using antiangiogenic agents: Mechanistic insights, current progress, and clinical challenges. *Cancer Commun.* **41**, 830–850 (2021).
8. M. E. Fane *et al.*, sFRP2 supersedes VEGF as an age-related driver of angiogenesis in melanoma, affecting response to anti-VEGF therapy in older patients. *Clin. Cancer Res.* **26**, 5709–5719 (2020).
9. P. Mabetta, Paradigms of vascularization in melanoma: Clinical significance and potential for therapeutic targeting. *Biomed. Pharmacother.* **127**, 110135 (2020).
10. P. Salven, P. Heikkilä, H. Joensuu, Enhanced expression of vascular endothelial growth factor in metastatic melanoma. *Br. J. Cancer* **76**, 930–934 (1997).
11. R. S. Apte, D. S. Chen, N. Ferrara, VEGF in signaling and disease: Beyond discovery and development. *Cell* **176**, 1248–1264 (2019).
12. K. B. Kim *et al.*, BEAM: A randomized phase II study evaluating the activity of bevacizumab in combination with carboplatin plus paclitaxel in patients with previously untreated advanced melanoma. *J. Clin. Oncol.* **30**, 34–41 (2012).
13. K. A. Varker *et al.*, A randomized phase 2 trial of bevacizumab with or without daily low-dose interferon alfa-2b in metastatic malignant melanoma. *Ann. Surg. Oncol.* **14**, 2367–2376 (2007).
14. P. G. Corrie *et al.*, Adjuvant bevacizumab in patients with melanoma at high risk of recurrence (AVAST-M): Preplanned interim results from a multicentre, open-label, randomised controlled phase 3 study. *Lancet Oncol.* **15**, 620–630 (2014).
15. P. G. Corrie *et al.*, Adjuvant bevacizumab for melanoma patients at high risk of recurrence: Survival analysis of the AVAST-M trial. *Ann. Oncol.* **29**, 1843–1852 (2018).
16. M. R. Girotti, M. Salatino, T. Dalotto-Moreno, G. A. Rabinovich, Sweetening the hallmarks of cancer: Galectins as multifunctional mediators of tumor progression. *J. Exp. Med.* **217**, e20182041 (2020).
17. P. Navarro, N. Martínez-Bosch, A. G. Blidner, G. A. Rabinovich, Impact of galectins in resistance to anticancer therapies. *Clin. Cancer Res.* **26**, 6086–6101 (2020).
18. D. K. Nambiar *et al.*, Galectin-1-driven T cell exclusion in the tumor endothelium promotes immunotherapy resistance. *J. Clin. Invest.* **129**, 5553–5567 (2019).
19. D. O. Croci *et al.*, Glycosylation-dependent lectin-receptor interactions preserve angiogenesis in anti-VEGF refractory tumors. *Cell* **156**, 744–758 (2014).
20. P. Carabias *et al.*, Galectin-1 confers resistance to doxorubicin in hepatocellular carcinoma cells through modulation of P-glycoprotein expression. *Clin. Death Dis.* **13**, 79 (2022).
21. P. Kuo *et al.*, Galectin-1 mediates radiation-related lymphopenia and attenuates NSCLC radiation response. *Clin. Cancer Res.* **20**, 5558–5569 (2014).
22. M. B. Fuentes *et al.*, Regulated expression of galectin-1 during T-cell activation involves Lck and Fyn kinases and signaling through MEK1/ERK, p38 MAP kinase and p70S6 kinase. *Mol. Cell. Biochem.* **267**, 177–185 (2004).
23. J. M. Ilarregui, G. A. Bianco, M. A. Toscano, G. A. Rabinovich, The coming of age of galectins as immunomodulatory agents: Impact of these carbohydrate binding proteins in T cell physiology and chronic inflammatory disorders. *Ann. Rheum. Dis.* **64**, iv96–iv103 (2005).
24. M. A. Toscano *et al.*, Differential glycosylation of TH1, TH2 and TH-17 effector cells selectively regulates susceptibility to cell death. *Nat. Immunol.* **8**, 825–834 (2007).
25. G. A. Rabinovich *et al.*, Recombinant galectin-1 and its genetic delivery suppress collagen-induced arthritis via T cell apoptosis. *J. Exp. Med.* **190**, 385–397 (1999).
26. S. R. Stowell *et al.*, Galectin-1, -2, and -3 exhibit differential recognition of sialylated glycans and blood group antigens. *J. Biol. Chem.* **283**, 10109–10123 (2008).
27. T. Dalotto-Moreno *et al.*, Targeting galectin-1 overcomes breast cancer-associated immunosuppression and prevents metastatic disease. *Cancer Res.* **73**, 1107–1117 (2013).
28. A. J. Cagnoni *et al.*, Galectin-1 fosters an immunosuppressive microenvironment in colorectal cancer by reprogramming CD8+ regulatory T cells. *Proc. Natl. Acad. Sci. U.S.A.* **118**, e2102950118 (2021).
29. J. M. Ilarregui *et al.*, Tolerogenic signals delivered by dendritic cells to T cells through a galectin-1-driven immunoregulatory circuit involving interleukin 27 and interleukin 10. *Nat. Immunol.* **10**, 981–991 (2009).
30. N. Rubinstein *et al.*, Targeted inhibition of galectin-1 gene expression in tumor cells results in heightened T cell-mediated rejection: A potential mechanism of tumor-immune privilege. *Cancer Cell* **5**, 241–251 (2004).
31. F. Cedeno-Laurent, M. Opperman, S. R. Barthel, V. K. Kuchroo, C. J. Dimitroff, Galectin-1 triggers an immunoregulatory signature in Th cells functionally defined by IL-10 expression. *J. Immunol.* **188**, 3127–3137 (2012).
32. V. L. J. Thijssen *et al.*, Galectin-1 is essential in tumor angiogenesis and is a target for antiangiogenesis therapy. *Proc. Natl. Acad. Sci. U.S.A.* **103**, 15975–15980 (2006).
33. V. L. Thijssen *et al.*, Tumor cells secrete galectin-1 to enhance endothelial cell activity. *Cancer Res.* **70**, 6216–6224 (2010).
34. D. O. Croci *et al.*, Disrupting galectin-1 interactions with N-glycans suppresses hypoxia-driven angiogenesis and tumorigenesis in Kaposi's sarcoma. *J. Exp. Med.* **209**, 1985–2000 (2012).
35. S. H. Hsieh *et al.*, Galectin-1, a novel ligand of neuropilin-1, activates VEGFR-2 signaling and modulates the migration of vascular endothelial cells. *Oncogene* **27**, 3746–3753 (2008).

36. M.-H. Wu *et al.*, Galectin-1 induces vascular permeability through the neuropilin-1/vascular endothelial growth factor receptor-1 complex. *Angiogenesis* **17**, 839–849 (2014).
37. F. S. Hodi *et al.*, Bevacizumab plus ipilimumab in patients with metastatic melanoma. *Cancer Immunol. Res.* **2**, 632–642 (2014).
38. X. Wu *et al.*, Combined anti-VEGF and anti-CTLA-4 therapy elicits humoral immunity to galectin-1 which is associated with favorable clinical outcomes. *Cancer Immunol. Res.* **5**, 446–454 (2017).
39. T. Urup *et al.*, Transcriptional changes induced by bevacizumab combination therapy in responding and non-responding recurrent glioblastoma patients. *BMC Cancer* **17**, 278 (2017).
40. J. M. Pérez Sáez *et al.*, Characterization of a neutralizing anti-human galectin-1 monoclonal antibody with angioregulatory and immunomodulatory activities. *Angiogenesis* **24**, 1–5 (2021).
41. M. Potente, H. Gerhardt, P. Carmeliet, Basic and therapeutic aspects of angiogenesis. *Cell* **146**, 873–887 (2011).
42. N. Ferrara, K. J. Hillan, H.-P. Gerber, W. Novotny, Discovery and development of bevacizumab, an anti-VEGF antibody for treating cancer. *Nat. Rev. Drug Discov.* **3**, 391–400 (2004).
43. D. Fukumura, J. Kloepper, Z. Amoozgar, D. G. Duda, R. K. Jain, Enhancing cancer immunotherapy using antiangiogenics: Opportunities and challenges. *Nat. Rev. Clin. Oncol.* **15**, 325–340 (2018).
44. G. C. Jayson, R. Kerbel, L. M. Ellis, A. L. Harris, Antiangiogenic therapy in oncology: Current status and future directions. *Lancet* **388**, 518–529 (2016).
45. H. Barrow *et al.*, Serum galectin-2, -4, and -8 are greatly increased in colon and breast cancer patients and promote cancer cell adhesion to blood vascular endothelium. *Clin. Cancer Res.* **17**, 7035–7046 (2011).
46. H. Barrow, J. M. Rhodes, L.-G. Yu, Simultaneous determination of serum galectin-3 and -4 levels detects metastases in colorectal cancer patients. *Cell. Oncol.* **36**, 9–13 (2013).
47. I. Iurisci *et al.*, Concentrations of galectin-3 in the sera of normal controls and cancer patients. *Clin. Cancer Res.* **6**, 1389–1393 (2000).
48. C. Chen *et al.*, Circulating galectins -2, -4 and -8 in cancer patients make important contributions to the increased circulation of several cytokines and chemokines that promote angiogenesis and metastasis. *Br. J. Cancer* **110**, 741–752 (2014).
49. J. Ouyang *et al.*, Galectin-1 serum levels reflect tumor burden and adverse clinical features in classical Hodgkin lymphoma. *Blood* **121**, 3431–3433 (2013).
50. M. Watanabe *et al.*, Clinical significance of circulating galectins as colorectal cancer markers. *Oncol. Rep.* **25**, 1217–1226 (2011).
51. N. Kaneko *et al.*, Potential tumor markers of renal cell carcinoma: α -Enolase for postoperative follow up, and galectin-1 and galectin-3 for primary detection. *Int. J. Urol.* **20**, 530–535 (2013).
52. S. Saussez *et al.*, Serum galectin-1 and galectin-3 levels in benign and malignant nodular thyroid disease. *Thyroid* **18**, 705–712 (2008).
53. T. Verschuere *et al.*, Altered galectin-1 serum levels in patients diagnosed with high-grade glioma. *J. Neurooncol.* **115**, 9–17 (2013).
54. K. Chen, Y. Cai, M. Zhang, Z. Wu, Y. Wu, Both serum and tissue Galectin-1 levels are associated with adverse clinical features in neuroblastoma. *Pediatr. Blood Cancer* **65**, e27229 (2018).
55. S. Aggarwal, S. C. Sharma, S. N. Das, Galectin-1 and galectin-3: Plausible tumour markers for oral squamous cell carcinoma and suitable targets for screening high-risk population. *Clin. Chim. Acta* **442**, 13–21 (2015).
56. S. Saussez *et al.*, The determination of the levels of circulating galectin-1 and -3 in HNSCC patients could be used to monitor tumor progression and/or responses to therapy. *Oral Oncol.* **44**, 86–93 (2008).
57. V. Arcolia *et al.*, Galectin-1 is a diagnostic marker involved in thyroid cancer progression. *Int. J. Oncol.* **51**, 760–770 (2017).
58. M. J. Carlini *et al.*, Clinical relevance of galectin-1 expression in non-small cell lung cancer patients. *Lung Cancer* **84**, 73–78 (2014).
59. N. Martínez-Bosch *et al.*, Increased plasma levels of galectin-1 in pancreatic cancer: Potential use as biomarker. *Oncotarget* **9**, 32984–32996 (2018).
60. S. P. Méndez-Huergo, A. G. Blidner, G. A. Rabinovich, Galectins: Emerging regulatory checkpoints linking tumor immunity and angiogenesis. *Curr. Opin. Immunol.* **45**, 8–15 (2017).
61. S. Di Lella *et al.*, When galectins recognize glycans: From biochemistry to physiology and back again. *Biochemistry* **50**, 7842–7857 (2011).
62. C. M. Guardia *et al.*, Structural basis of redox-dependent modulation of galectin-1 dynamics and function. *Glycobiology* **24**, 428–441 (2014).
63. C. M. John, H. Leffler, B. Kahl-Knutsson, I. Svensson, G. A. Jarvis, Truncated galectin-3 inhibits tumor growth and metastasis in orthotopic nude mouse model of human breast cancer. *Clin. Cancer Res.* **9**, 2374 (2003).
64. S. R. Sangeetha, P. S. Appukkuttan, IgA1 is the premier serum glycoprotein recognized by human galectin-1 since T antigen (Gal β 1 \rightarrow 3GalNAc) is far superior to non-repeating N-acetyl lactosamine as ligand. *Int. J. Biol. Macromol.* **35**, 269–276 (2005).
65. O. Roda *et al.*, Galectin-1 is a novel functional receptor for tissue plasminogen activator in pancreatic cancer. *Gastroenterology* **136**, 1379–1390.e5 (2009).
66. B. T. Maybruck, L. W. Pfannenstiel, M. Diaz-Montero, B. R. Gastman, Tumor-derived exosomes induce CD8(+) T cell suppressors. *J. Immunother. Cancer* **5**, 65 (2017).
67. M. J. Kailemia *et al.*, Recent advances in the mass spectrometry methods for glycomics and cancer. *Anal. Chem.* **90**, 208–224 (2018).
68. J. Goveia *et al.*, An integrated gene expression landscape profiling approach to identify lung tumor endothelial cell heterogeneity and angiogenic candidates. *Cancer Cell* **37**, 21–36.e13 (2020).
69. J. J. García-Vallejo *et al.*, Activation of human endothelial cells by tumor necrosis factor- α results in profound changes in the expression of glycosylation-related genes. *J. Cell. Physiol.* **206**, 203–210 (2006).
70. W. Luo *et al.*, Identification of galectin-1 as a novel mediator for chemoresistance in chronic myeloid leukemia cells. *Oncotarget* **7**, 26709–26723 (2016).
71. C. A. Orozco *et al.*, Targeting galectin-1 inhibits pancreatic cancer progression by modulating tumor-stroma crosstalk. *Proc. Natl. Acad. Sci. U.S.A.* **115**, 3769–3778 (2018).
72. P. Storti *et al.*, Galectin-1 suppression delineates a new strategy to inhibit myeloma-induced angiogenesis and tumoral growth in vivo. *Leukemia* **30**, 2351–2363 (2016).
73. C.-C. Yeh *et al.*, Integrated stable isotope labeling by amino acids in cell culture (SILAC) and isobaric tags for relative and absolute quantitation (iTRAQ) quantitative proteomic analysis identifies galectin-1 as a potential biomarker for predicting sorafenib resistance. *Mol. Cell. Proteomics* **14**, 1527–1545 (2015).
74. J. Ouyang *et al.*, Viral induction and targeted inhibition of galectin-1 in EBV+ posttransplant lymphoproliferative disorders. *Blood* **117**, 4315–4322 (2011).
75. J. M. Lykken *et al.*, Galectin-1 drives lymphoma CD20 immunotherapy resistance: Validation of a preclinical system to identify resistance mechanisms. *Blood* **127**, 1886–1895 (2016).
76. M. Van Woensel *et al.*, Sensitization of glioblastoma tumor micro-environment to chemo- and immunotherapy by Galectin-1 intranasal knock-down strategy. *Sci. Rep.* **7**, 1217 (2017).
77. N. Bannoud *et al.*, Untangling galectin-mediated circuits that control hypoxia-driven angiogenesis. *Methods Mol. Biol.* **2442**, 635–653 (2022).
78. J. Schindelin *et al.*, Fiji: An open-source platform for biological-image analysis. *Nat. Methods* **9**, 676–682 (2012).